# Organic and polymeric photorefractive materials and devices

(Chapter 19)

Oksana Ostroverkhova

*Introduction to Organic Electronic and Optoelectronic Materials and Devices (Eds. Sun & Dalton)* CRC Press, 2008. ISBN-10: 0849392845

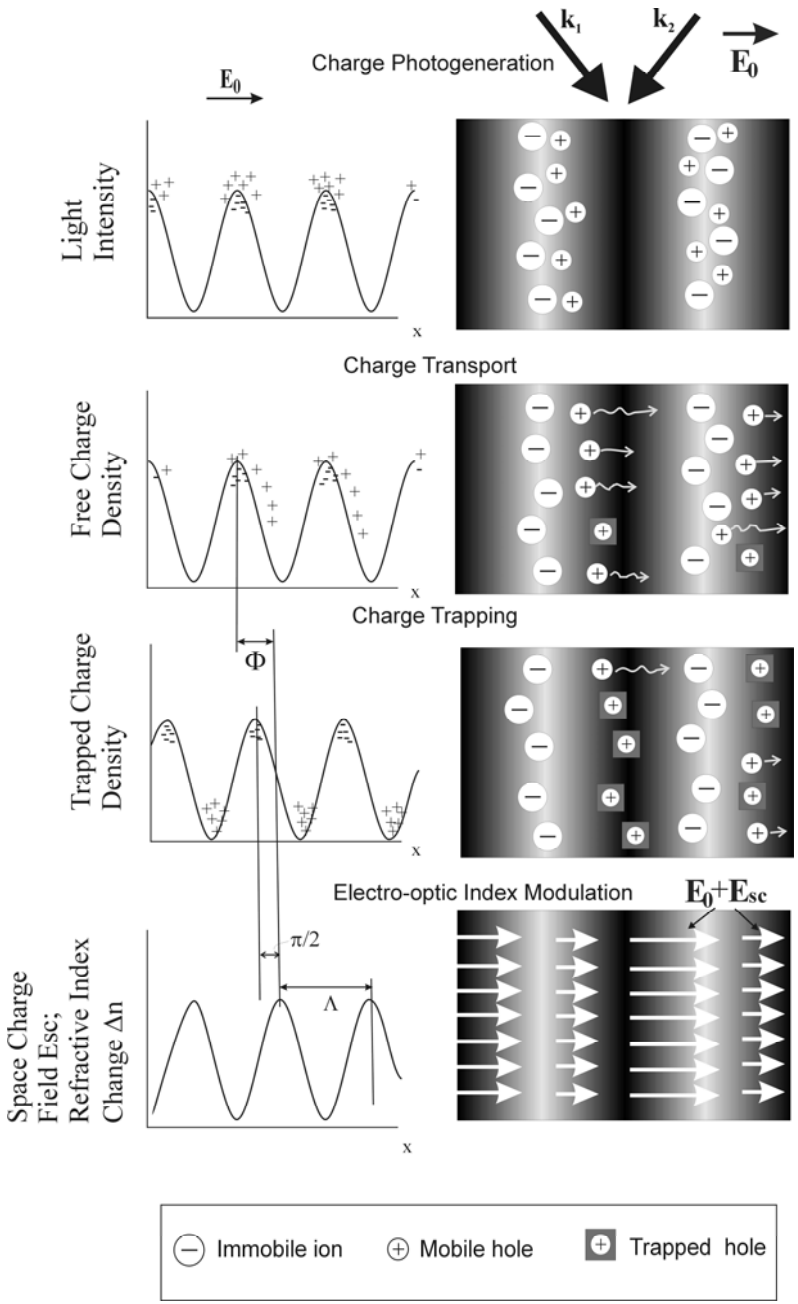


**Figure 19.1**. Photorefractive grating formation: (a) charge photogeneration; (b) charge transport; (c) charge trapping; (d) space-charge field formation and refractive index modulation.

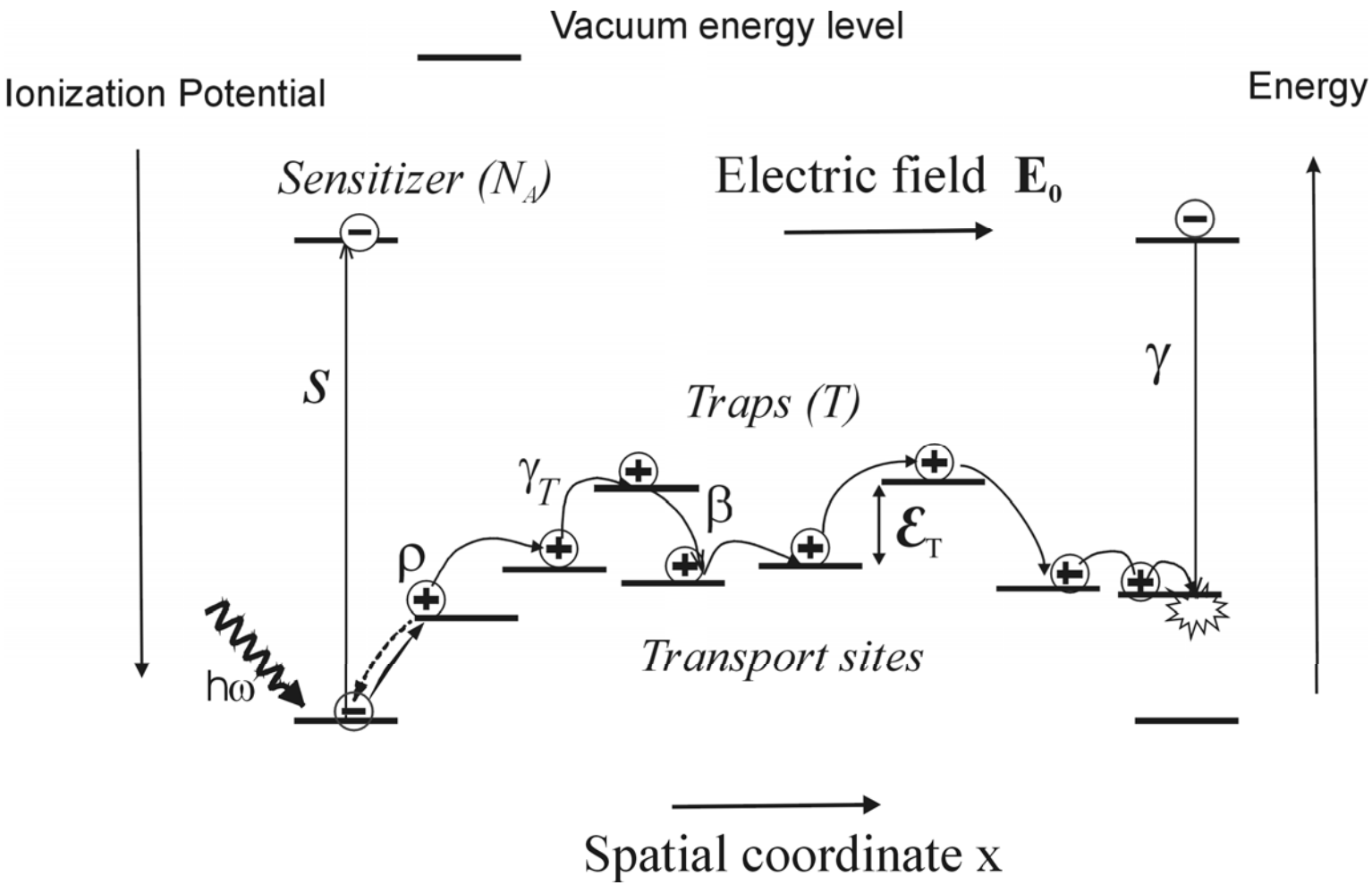


**Figure 19.2**. Schematic representation of the molecular model describing space-charge field formation in PR organic materials.

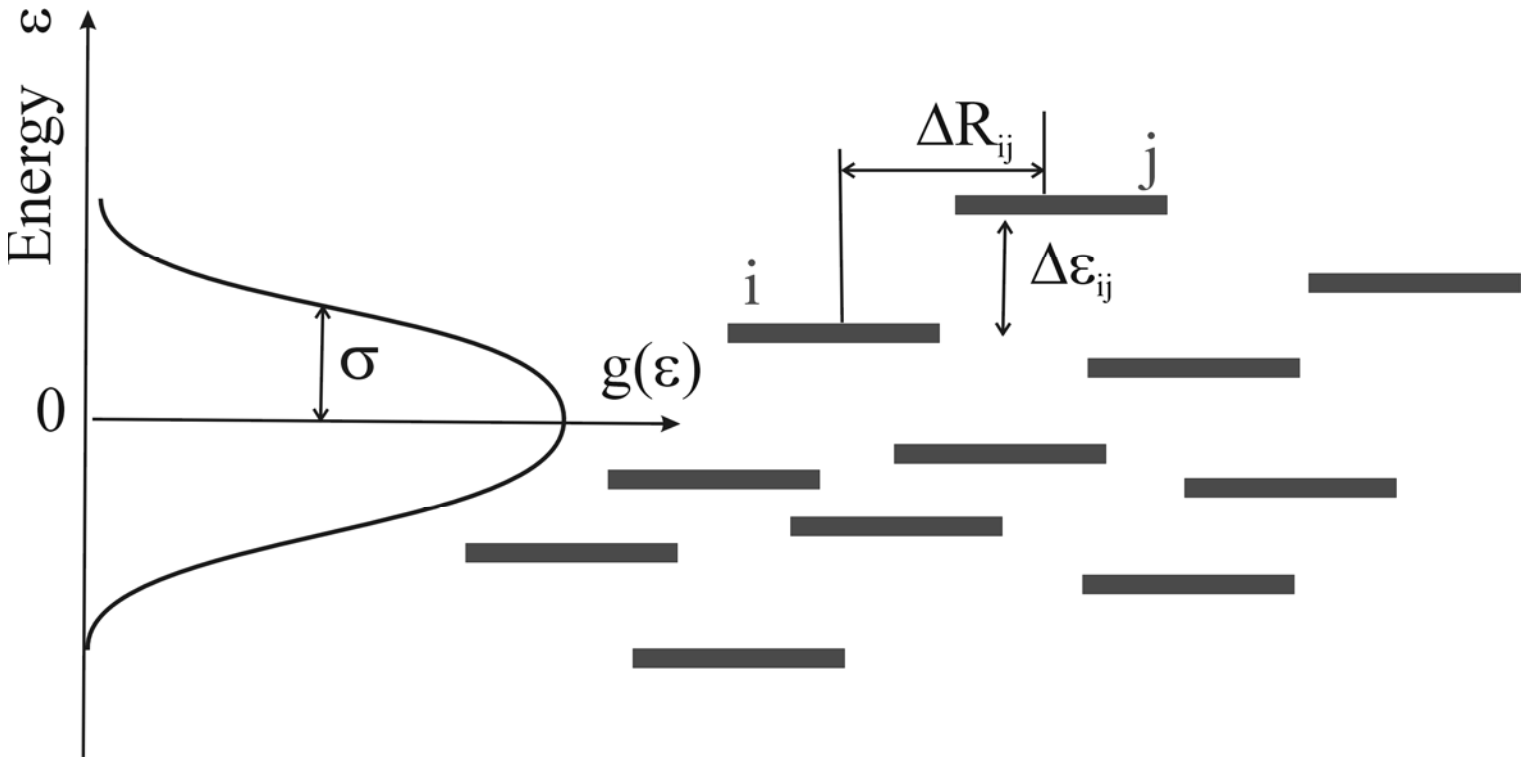


**Figure 19.3** Schematic representation of the charge transport manifold in PR polymers.

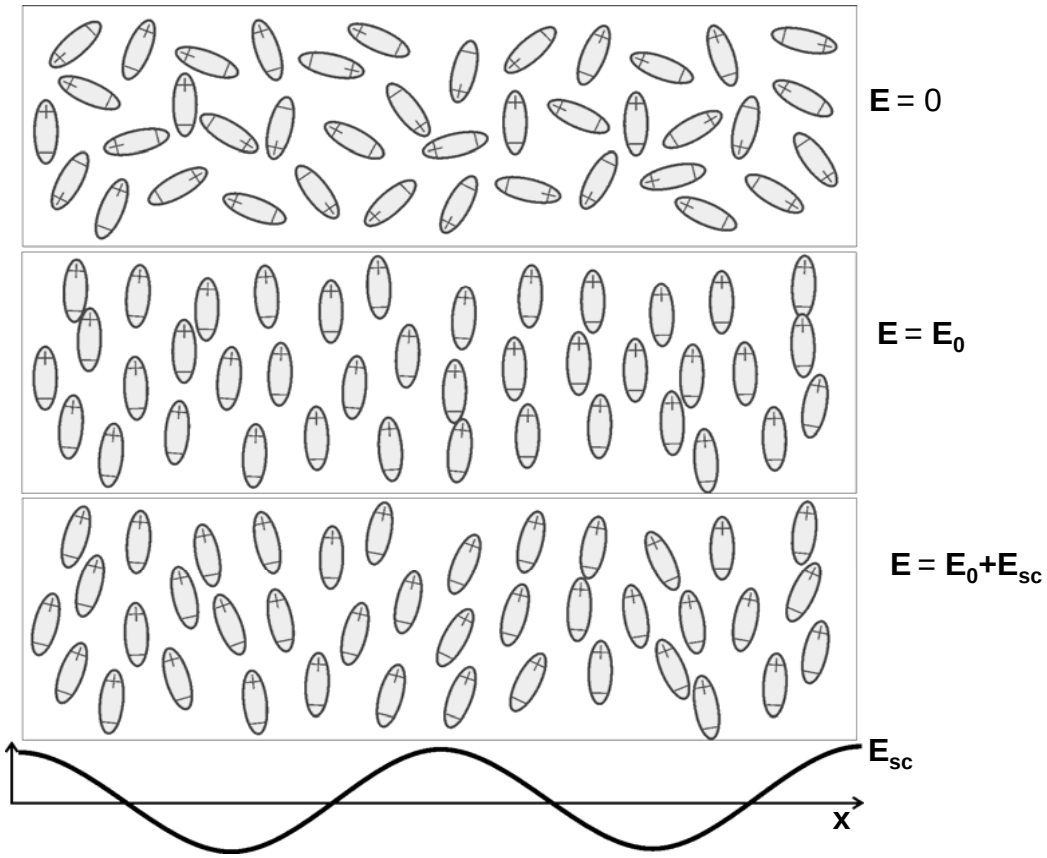


**Figure 19.4**. Chromophore orientation in the electric field: (a) no electric field; (b) electric field $\mathbf{E_0}$ is applied; (c) spatially-modulated space-charge field $\mathbf{E_{sc}}$ is added to the applied field.

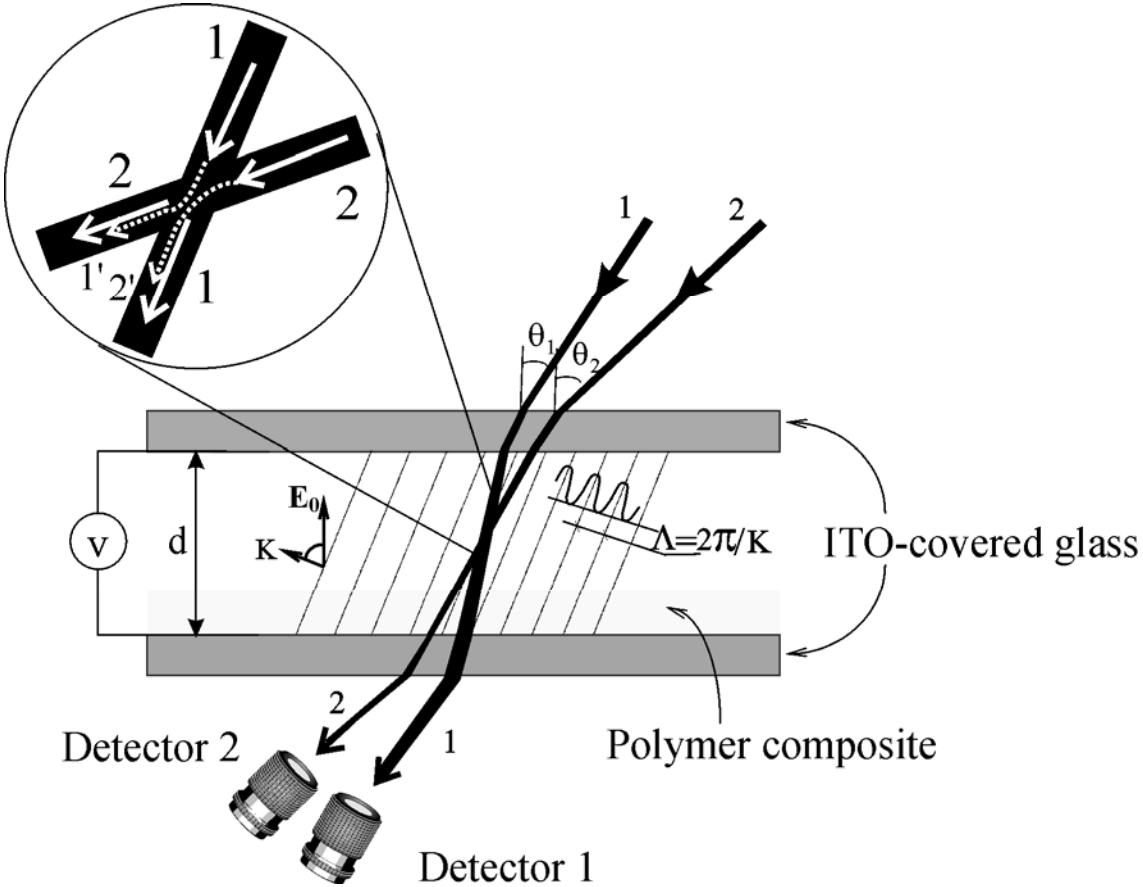


**Figure 19.5**. Experimental configuration used in two-beam coupling geometry.

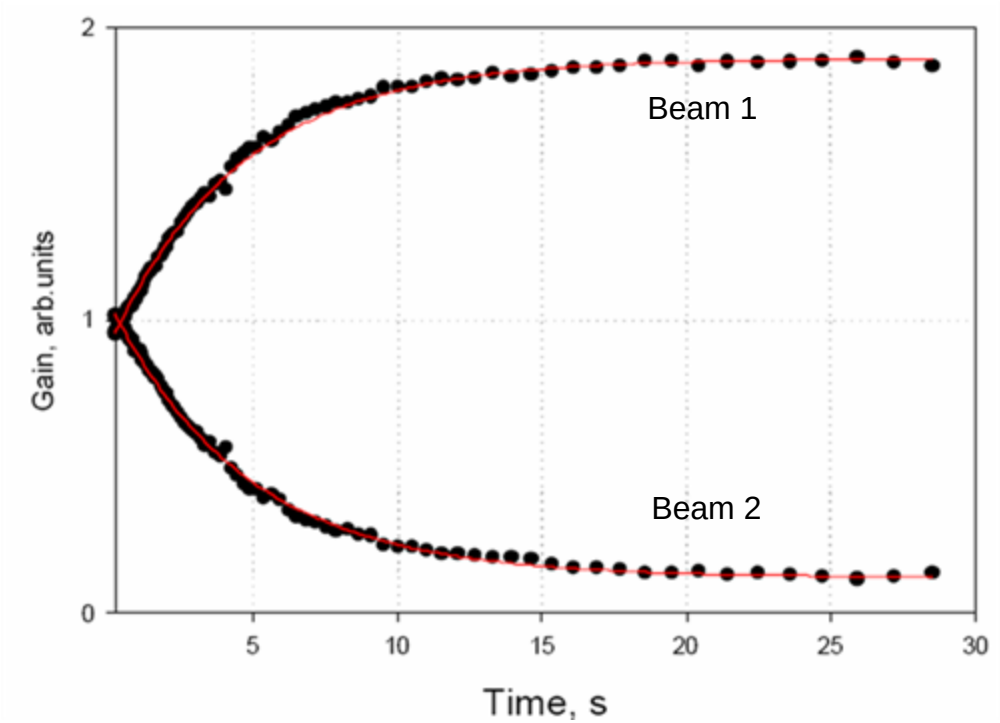


**Figure 19.6.** Typical experimental data obtained in two-beam coupling experiment in high-performance PR organic material. Almost complete energy transfer from beam 2 to beam 1 is achieved.

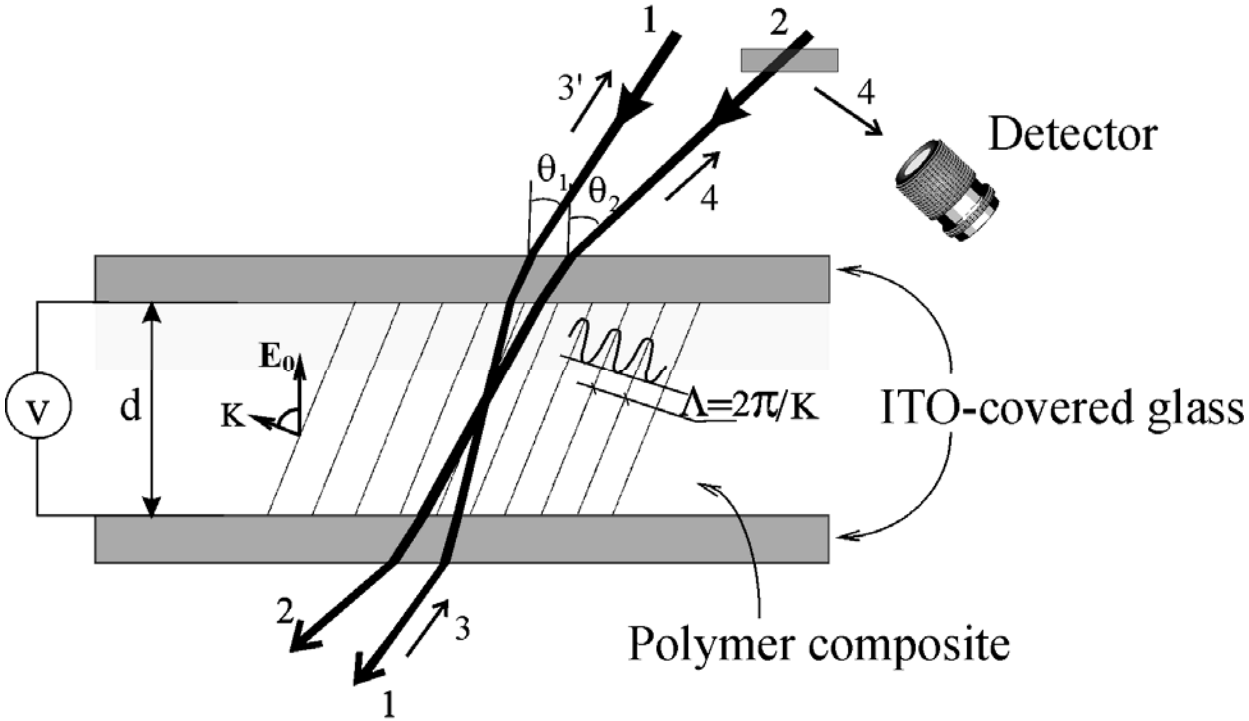


**Figure 19.7**. Experimental configuration used in four-wave-mixing geometry.

(a)

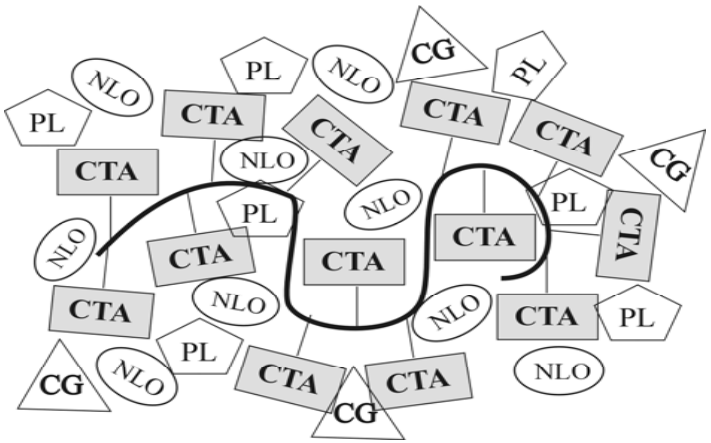


(b)

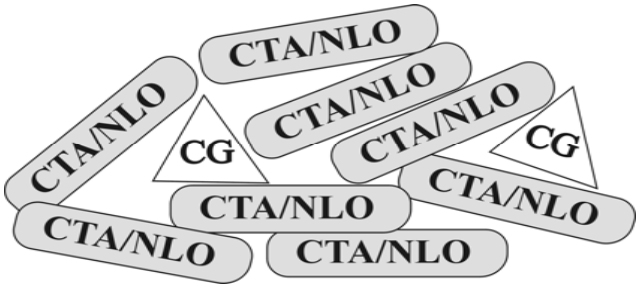


**Figure 19.8**. Typical content of a: (a) PR polymer composite and (b) PR organic amorphous glass. The notations are: CTA – charge transport agent, CG – charge generator, NLO – nonlinear optical chromophore, PL – plasticizer.

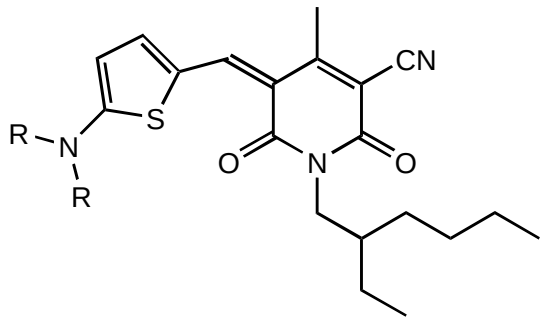


**ATOP-4**: R= $CH_2CH_2CH_3$

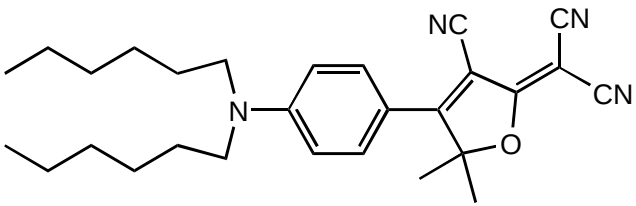


**DCDHF-6**

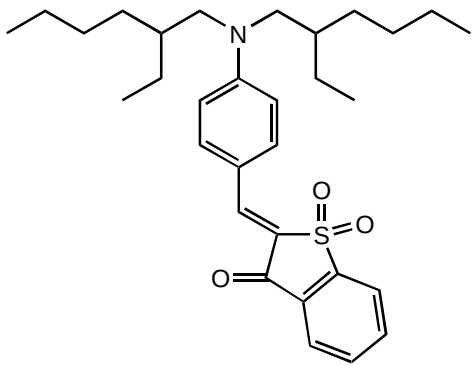


**Methine A**

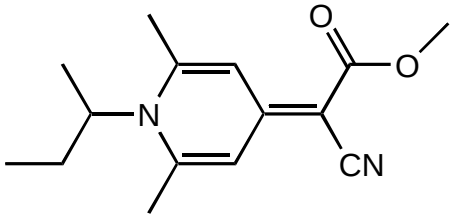


**2BNCM**

**Figure 19.9**. High-performance glass-forming molecules.

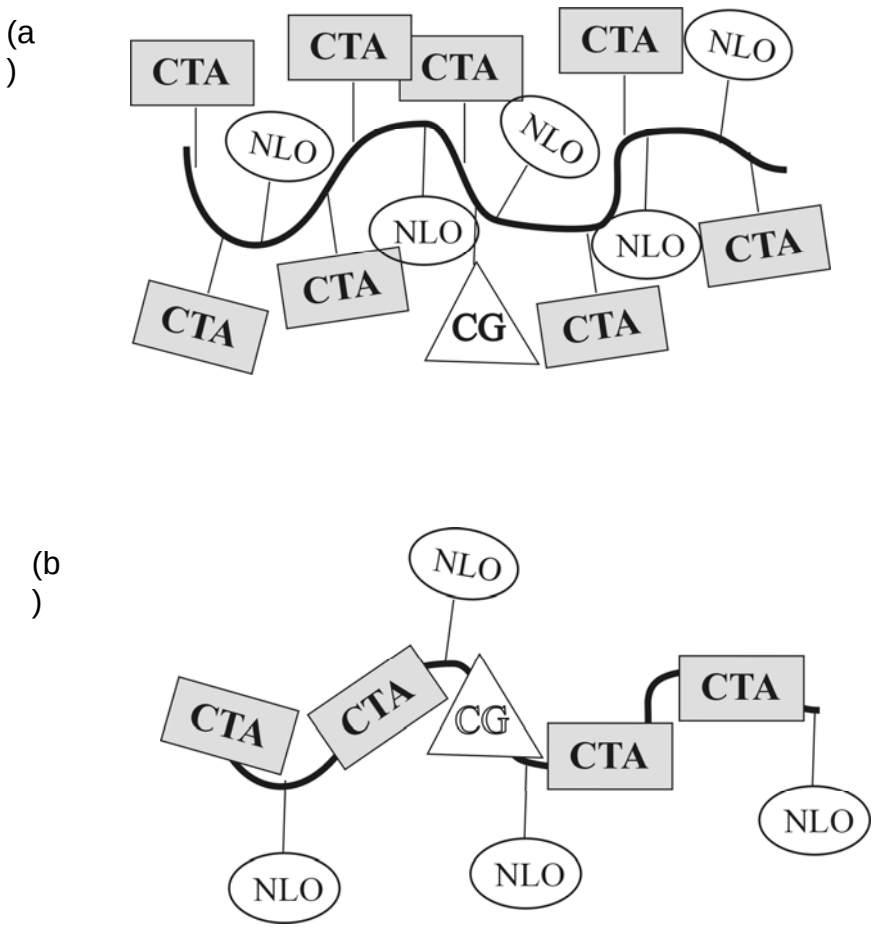


**Figure 19.10**. Examples of design of fully functionalized PR polymers : (a) inert polymer backbone with functional side groups; (b) photoconductive polymer backbone with NLO side groups. Notations are defined in Fig.8.

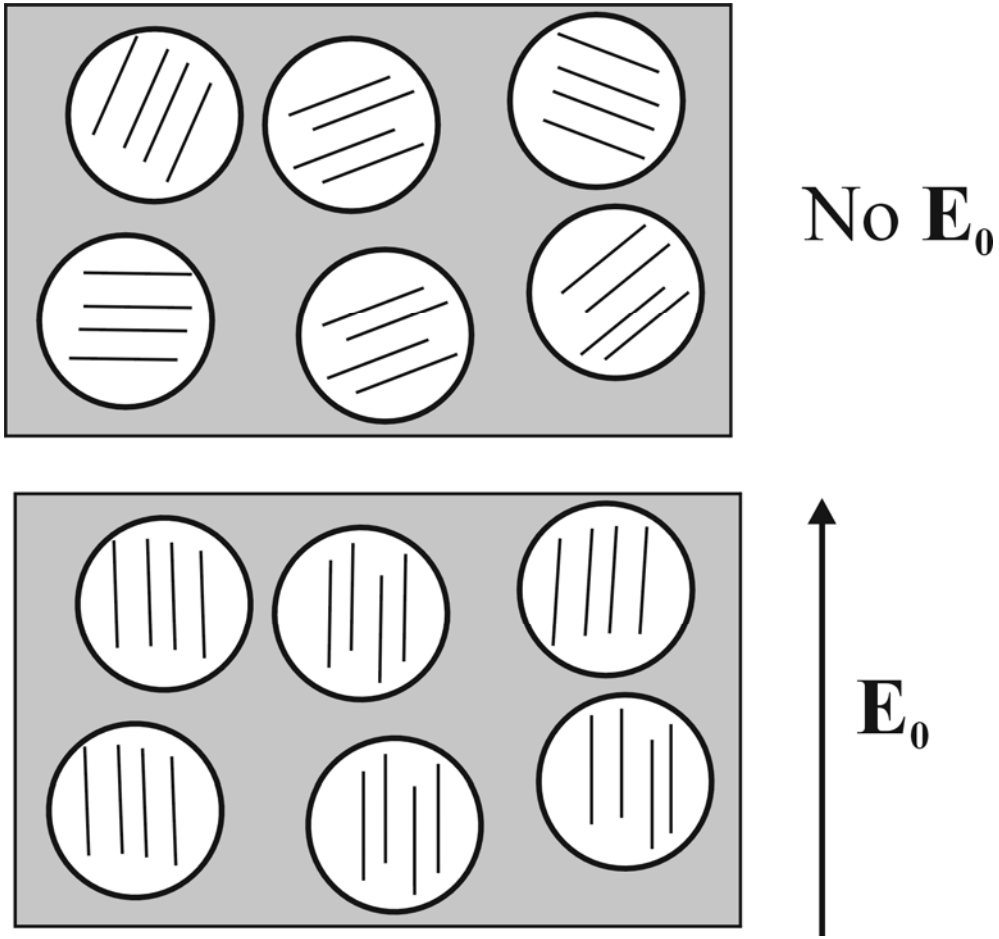


**Figure 19.11**. Schematics of the polymer-dispersed liquid crystals: liquid crystal droplets in a polymer matrix. (a) no electric field is applied, and the liquid crystal molecules in different droplets are randomly oriented; (b) in the presence of the applied electric field $\mathbf{E_0}$, the molecules within the droplets align.

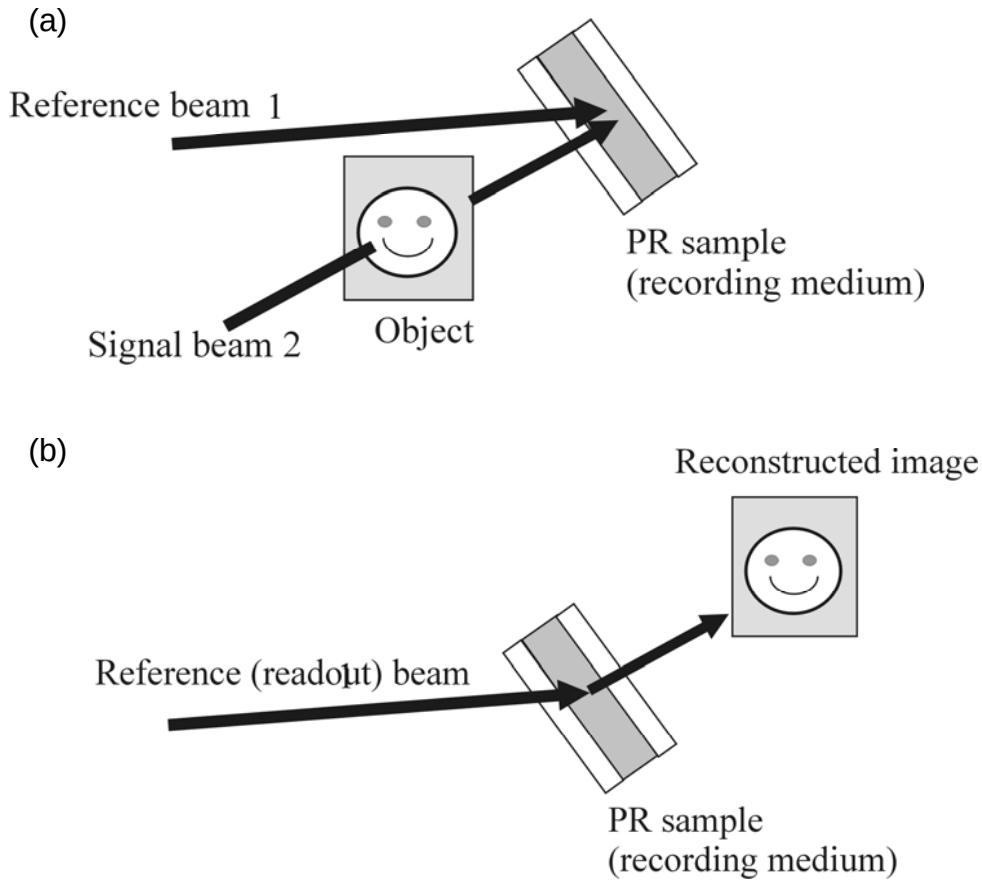


**Figure 19.12**. Holographic data storage using PR materials. (a) hologram recording; (b) hologram retrieving.

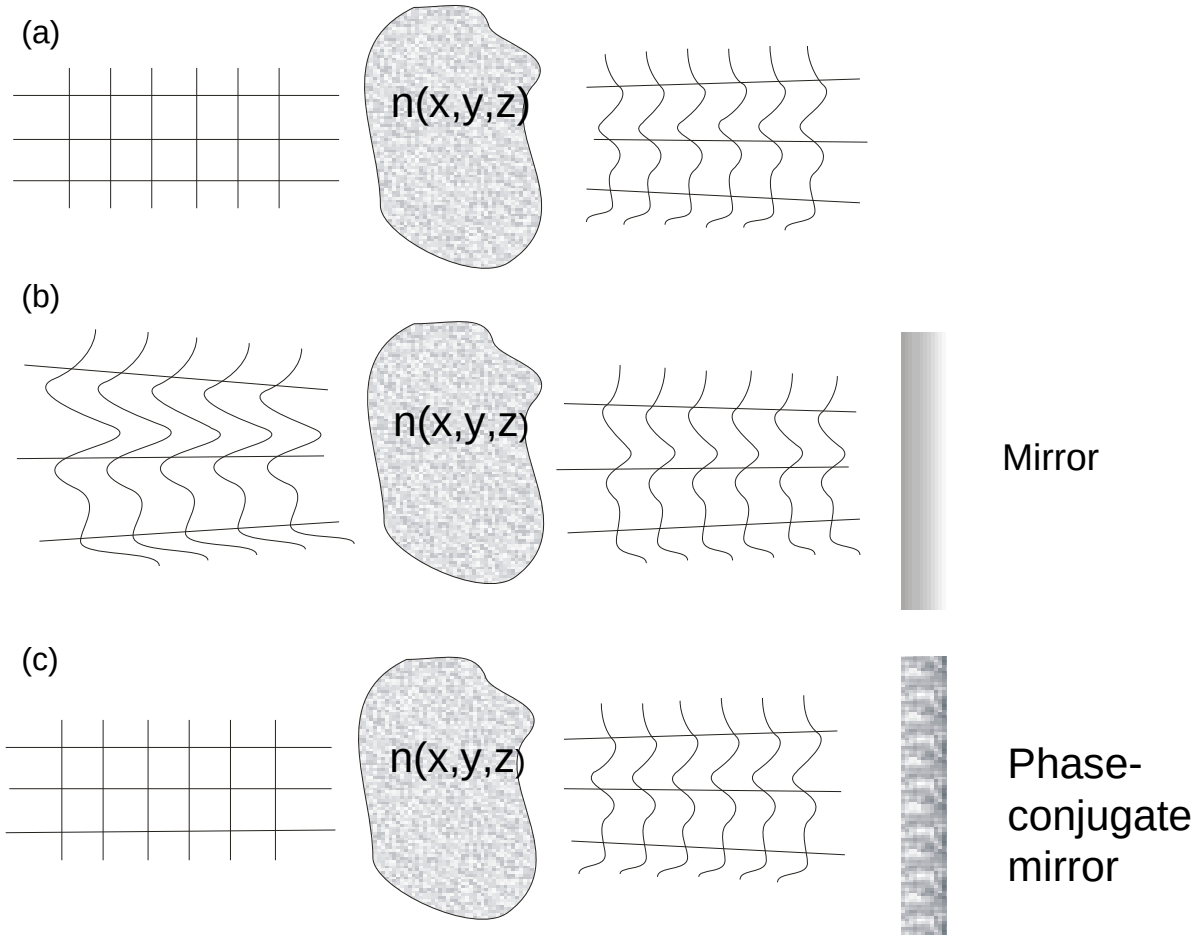


**Figure 19.13.** Concept of a phase conjugate mirror: (a) plane wave front distortion in a light beam passing through a transparent but inhomogeneous medium; (b) back-reflected wave from an ordinary mirror – wave front distortion accumulates on a return pass; (c) back-reflected wave from a phase-conjugate mirror – plane wave front is reconstructed on a return pass.

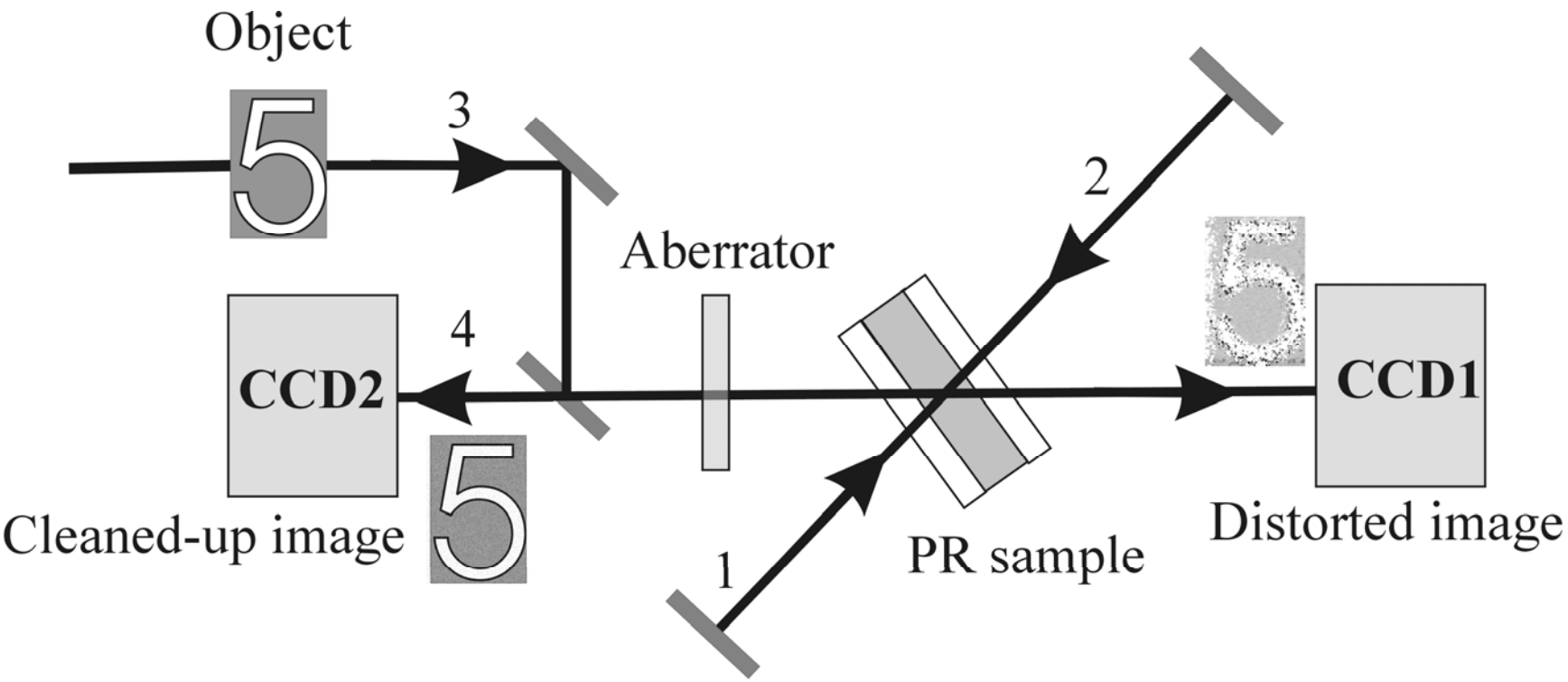


**Figure 19.14**. Experimental setup for the optical beam clean-up.

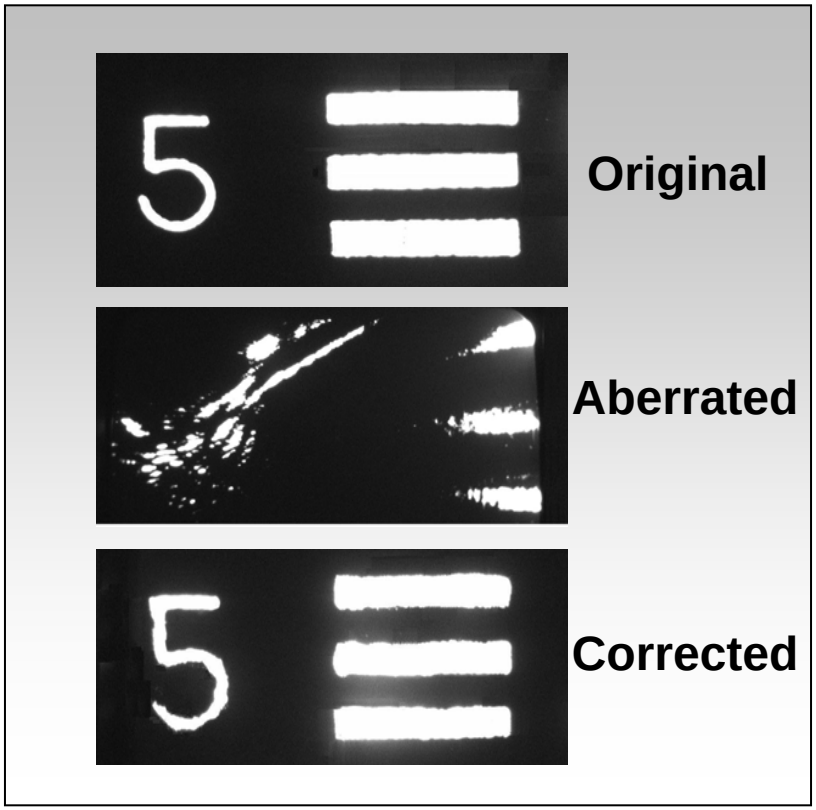


**Figure 19.15**. Correction of distorted images. (a) original object; (b) aberrated image of the object; (c) corrected image of the object.

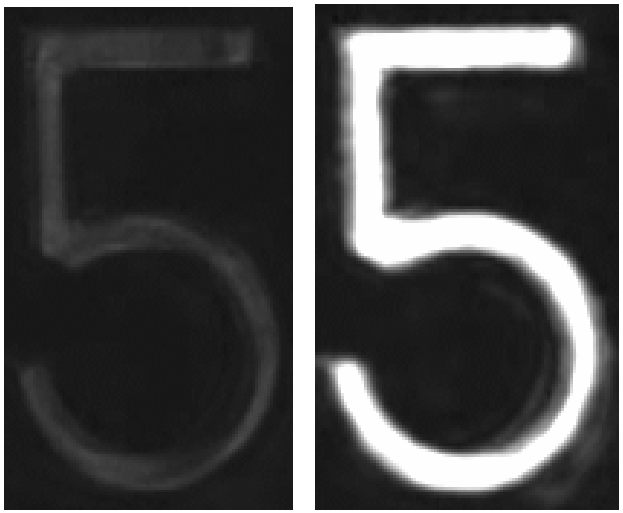

(a) (b)

**Figure 19.16**. Amplification of image of number 5 from the Air Force resolution test chart (68 mm line width) in PR polymer composite. Frame (a), the image in the absence of the reference beam and frame (b), amplified image 33 ms later.

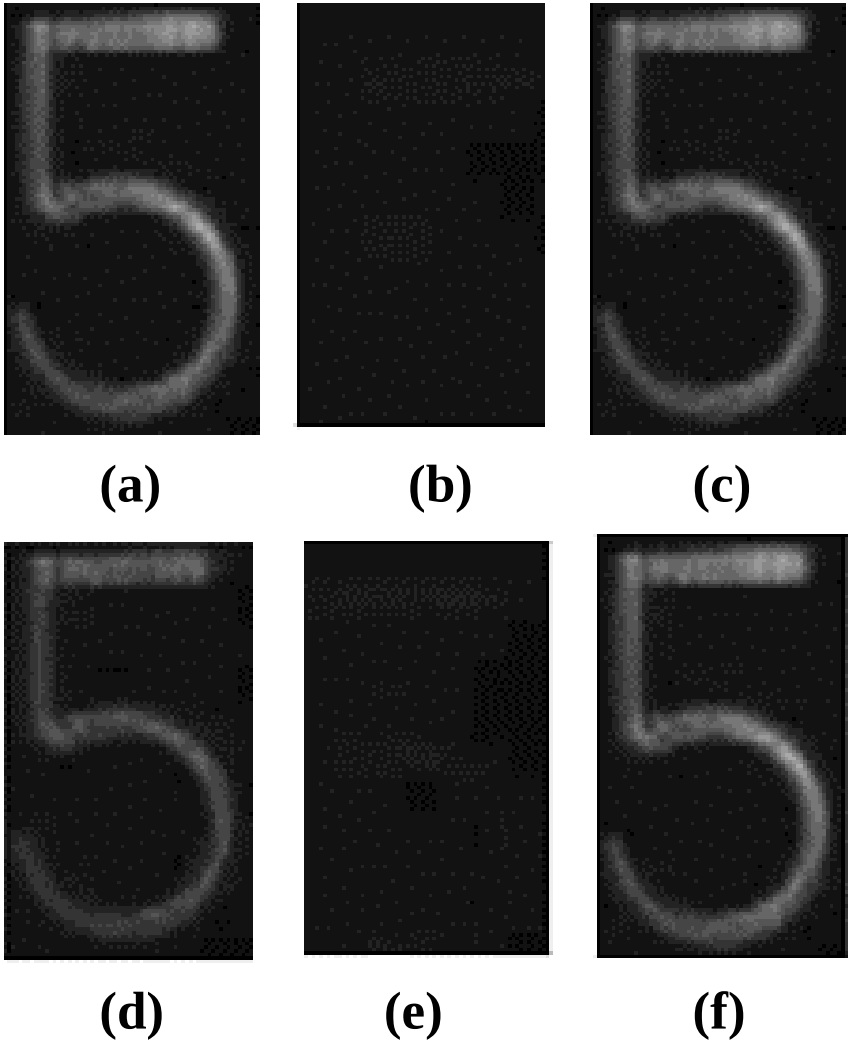


**Figure 19.17**. Demonstration of novelty filter effect using PR polymer composite. Frames: (a) Image with the reference beam off. (b) Image after the reference beam is on and steady state is reached; the output is dark. (c) After a sudden movement of the data mask, the image is visible. (d) Fading image after 1/30 s. (e) Back to a dark output after 4/30 s. (f) After the sudden movement of the data mask, the image is visible again.

(a)

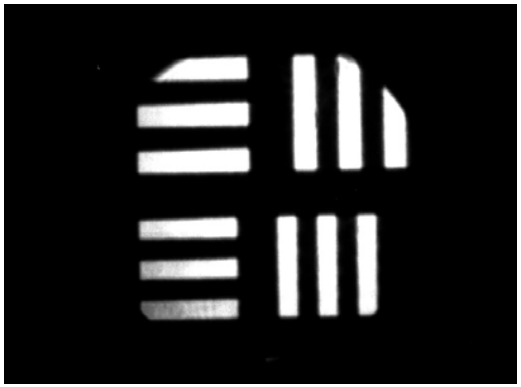

(b)

**Figure 19.18**. Demonstration of the edge enhancement effect using PR polymer composite. (a) With the ratio between the signal and reference beam intensities $I_{s0}/I_{r0}$ =0.1, the exact replica of the object is produced; (b) with the beam ratio $I_{s0}/I_{r0}$=20, the edge enhanced image is obtained.

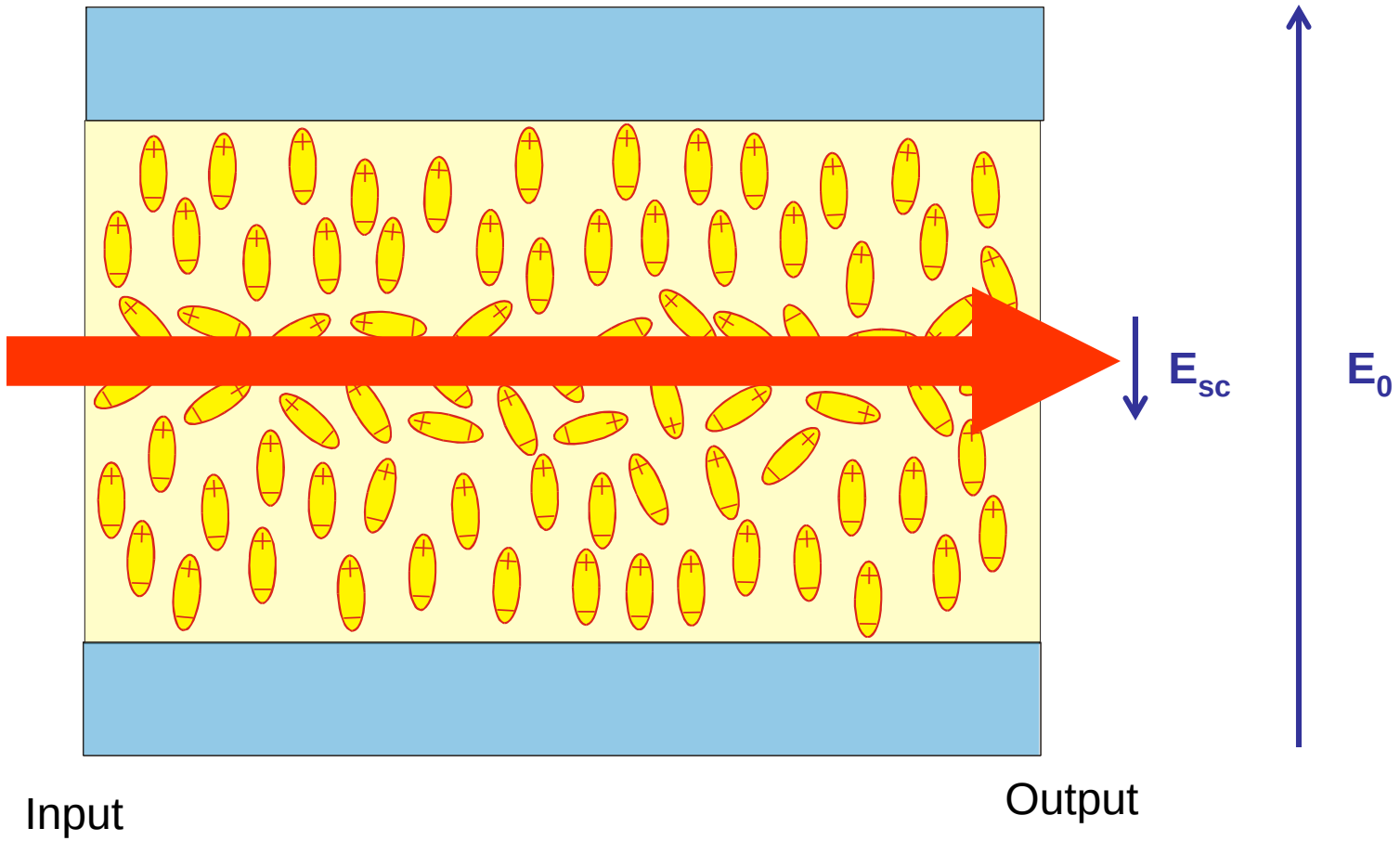


**Figure 19.19**. Mechanism of optically inducing refractive index profile in PR organic materials.

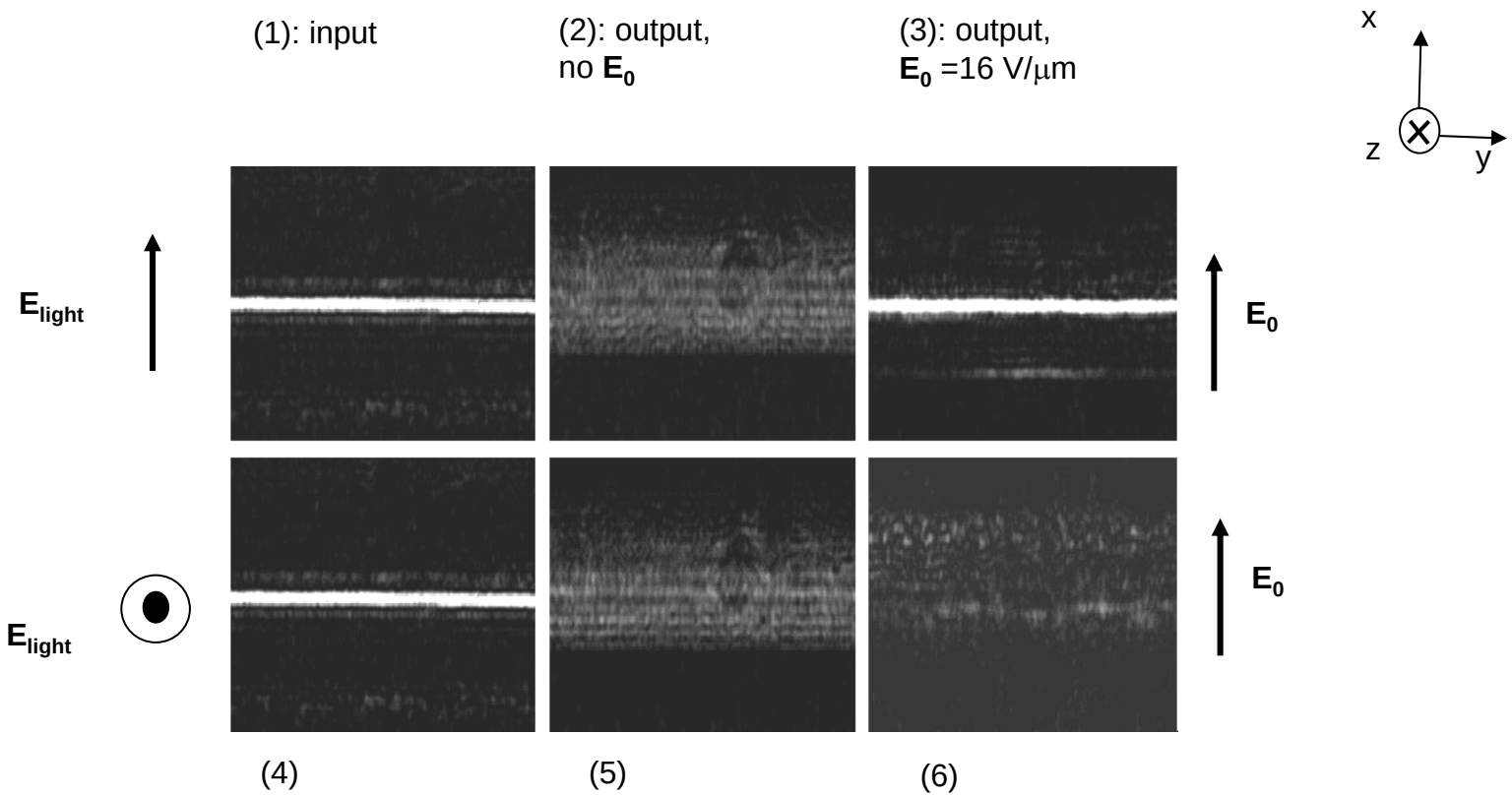


**Figure 19.20**. Observation of self-focusing and self-defocusing in a PR organic amorphous glass. Image of the beam at: frame (1) sample input (original y-polarized beam); (2) sample output ($E_0$=0; linearly diffracted y-polarized beam); (3) sample output ($E_0$=16 V/μm, self-trapped y-polarized beam); (4) sample input (original x-polarized beam); (5) sample output ($E_0$=0, linearly diffracted x-polarized beam); (6) sample output ($E_0$=16 V/μm, defocused x-polarized beam).

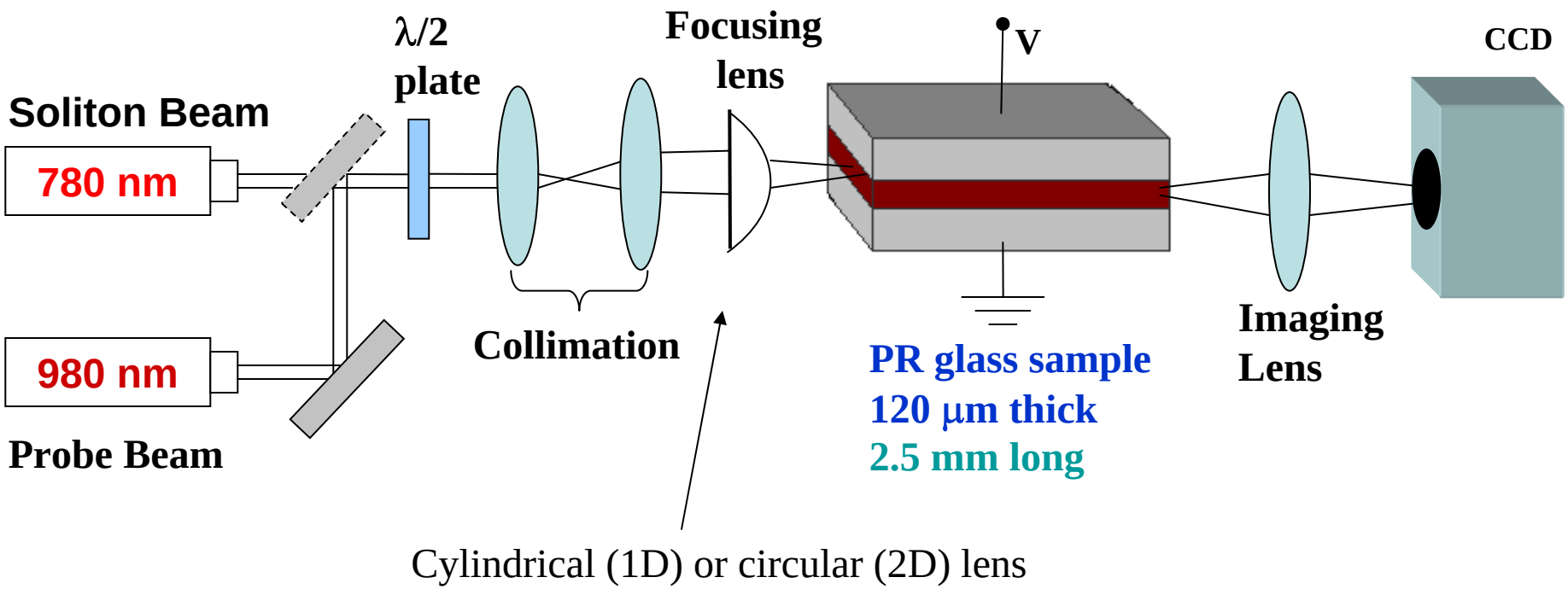


**Figure 19.21**. Experimental setup used for testing of the optically induced waveguide.

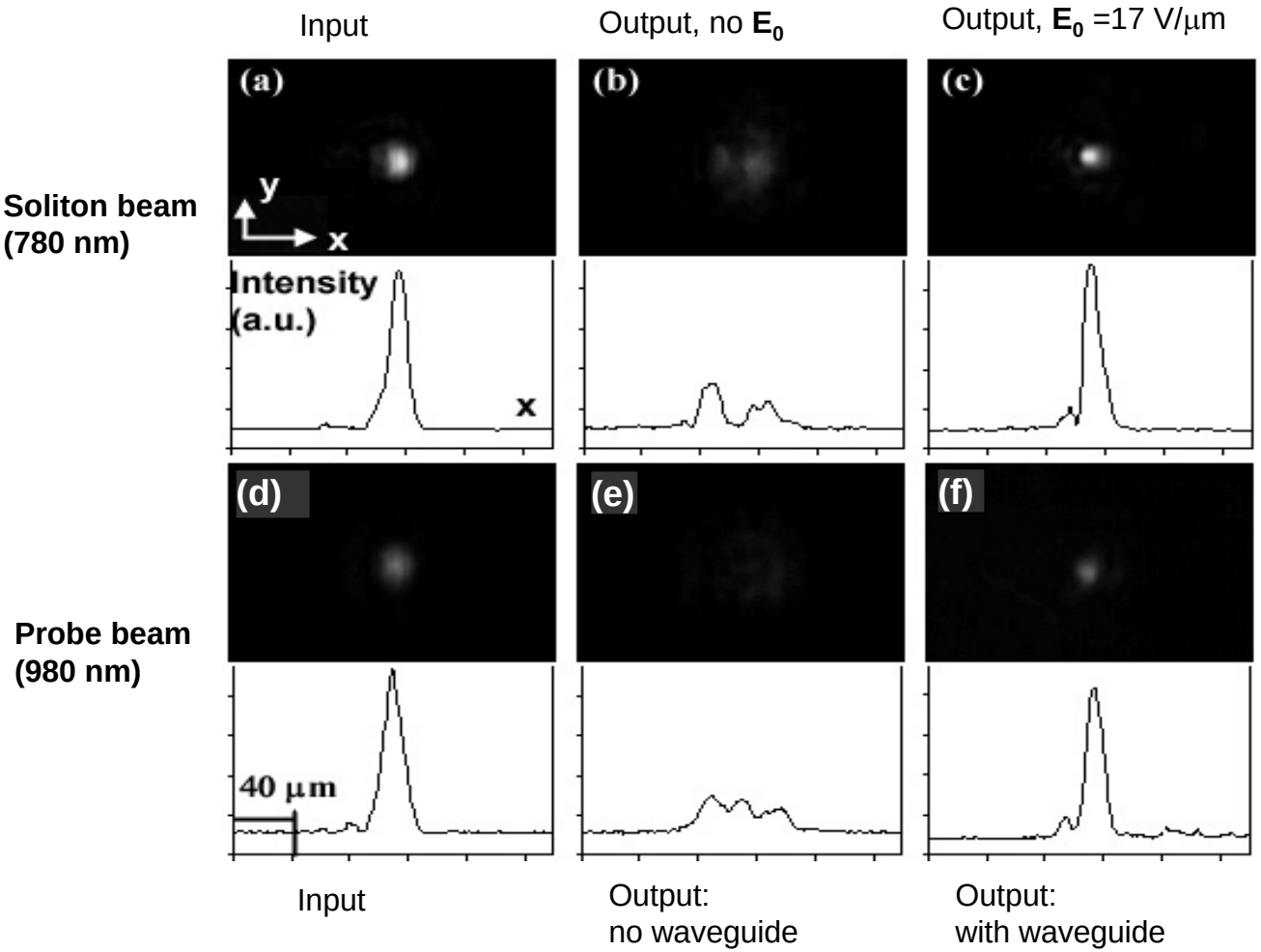


**Figure 19.22**. Circular waveguides induced by 2D solitons. Shown are transverse intensity patterns and beam profiles of the 780-nm (soliton) and 980-nm (probe) beams taken at the sample input (a, d) and output (b, c, e, f). Top: 780-nm soliton beam; Bottom: 980-nm probe beam. (b) soliton beam, no electric field, (c) soliton beam, $\mathbf{E_0}$ =17 V/μm, (e) probe beam, no waveguide (f) probe beam, in the presence of soliton beam-induced waveguide.

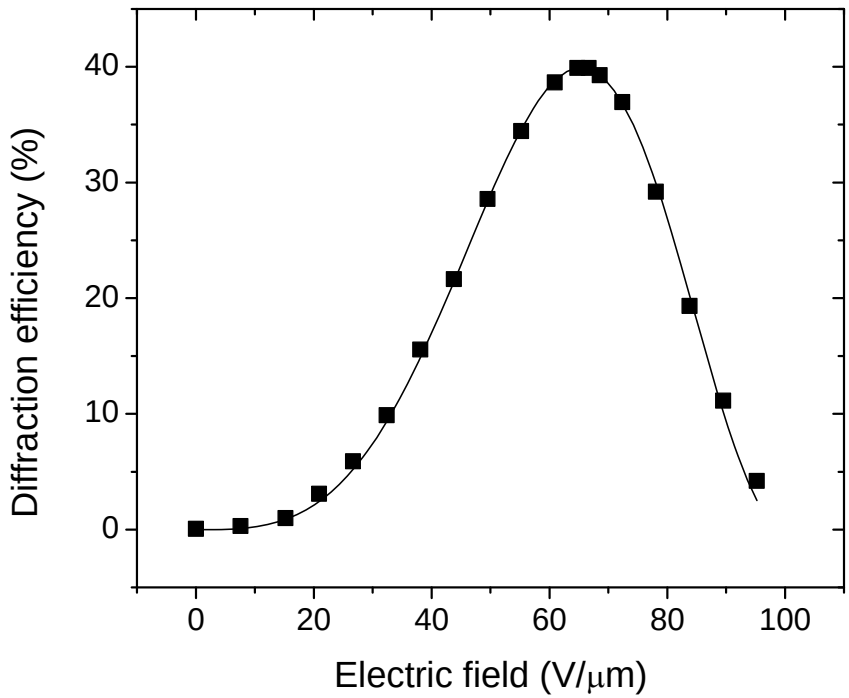


**Figure 19.23**. Diffraction efficiency as a function of electric field obtained in a PR polymer composite.